Originalarbeit

Elektrotech. Inftech. (2023) 140:324–337
https://doi.org/10.1007/s00502-023-01127-3

e+i elektrotechnik und informationstechnik

Optimum 7 MW HTS direct-drive wind turbine synchronous generator designs with different rotor and stator iron topologies

Robin Köster · Andreas Binder

Received: 25 November 2022 / Accepted: 31 January 2023 / Published online: 13 March 2023

Abstract Partially superconducting direct-drive wind turbine generators with high-temperature superconducting excitation winding enable an increase of the rated unit power, higher efficiency, and a high, adjustable power factor. The high excitation ampere-turns allow for iron topologies that differ from conventional permanent magnet-excited generators. This study compares four different iron topologies for 7 MW rated power and 8.33 rpm with a slotted stator or stator air gap winding regarding technical key characteristics and economic aspects. The generator designs are numerically optimized based on 2D finite element simulations. Maximum efficiency and the most lightweight designs are obtained with the stator air gap winding, whereas all-iron topologies prove advantageous regarding the trade-off between small active mass and high-temperature superconductor material consumption. The costs of the cryogenic cooling system and of the full converter are both found to be less than 15% for a wide range of generator designs.

Keywords Direct-drive wind turbine generators · High-temperature superconductors · Numerical optimization · Finite element simulation · Air gap winding

R. Köster (✉) · A. Binder
Institute of Electrical Energy Conversion,
Technical University of Darmstadt,
Landgraf-Georg-Str. 4, 64283 Darmstadt, Germany
r_koester@ew.tu-darmstadt.de

Optimierung von getriebelosen 7-MW-Windgeneratoren mit Hochtemperatur-Supraleiter-Erregerwicklung für verschiedene Generator-Topologien

Zusammenfassung Getriebelose Windgeneratoren mit supraleitender Erregerwicklung und normalleitender Statorwicklung ermöglichen die Steigerung der Nennleistung je Anlage sowie des Wirkungsgrads. Die verlustlose Gleichstromerregung ermöglicht es, den Leistungsfaktor zu variieren und gegenüber einer Permanentmagneterregung zu erhöhen. Mit supraleitenden Erregerwicklungen lassen sich zudem Topologien des Eisenkreises realisieren, die im Unterschied zu anderen Formen der Erregung weniger ferromagnetische Aktivteile für die Flussführung benötigen. Gegenstand dieser Untersuchung ist ein Vergleich von vier verschiedenen Topologien des Eisenkreises für einen Generator mit einer Nennleistung von 7 MW bei 8.33 min^{-1} unter technischen und ökonomischen Gesichtspunkten. Die verschiedenen Varianten werden basierend auf 2D-Finite-Elemente-Simulationen numerisch optimiert. Eine Topologie mit Stator-Luftspaltwicklung erweist sich als vorteilhaft hinsichtlich eines maximalen Wirkungsgrads und minimaler Aktivmasse, wohingegen Generatorvarianten mit einer Statorwicklung in Nuten und ferromagnetischem Polkern das größte Potenzial zur Reduktion der Aktivmasse bei minimalem Einsatz von Hochtemperatur-Supraleiter-Bandleitern bergen. Der auf das kryogene Kühlsystem und den Vollumrichter entfallende Kostenanteil beträgt für den größten Teil der Varianten weniger als 15 %.

Schlüsselwörter Getriebelose Windgeneratoren · Hochtemperatur-Supraleiter · Numerische Optimierung · Finite-Elemente-Simulation · Luftspaltwicklung

1 Introduction

The increase of wind turbines' rated unit power is an appropriate measure to reduce the installation cost for the production of renewable energy. Large wind turbines are preferably employed in offshore wind farms, where a low maintenance effort is mandatory for the used components [18]. Gearless direct-drive wind turbine solutions meet this requirement at the cost of very large, heavy generators with a huge material consumption, especially tons of expensive rare-earth magnets. The limiting factor of a restricted electromagnetic utilisation could be overcome by means of high temperature superconducting (HTS) excitation windings [3], which provide large excitation fields at small amount of HTS material, and/or allow for higher stator current loadings without need for flux-guiding iron teeth [7]. To date, the commercialisation of HTS excited direct-drive generators is hampered for economic reasons due to the high manufacturing costs of HTS tapes. Recent progress regarding the current carrying capacity (i.e. increase of critical current I_c by artificial pinning centers, APCs) and considerable cost reductions due to economies of scale may however yield solutions that are economically competitive to permanent magnet (PM) generators and may technically outperform these alternatives. The additional design degrees of freedom together with the more complex pole geometry imply optimum generator configurations that differ from PM excited generators (e.g. regarding the pole count). This work addresses this high-dimensional space of design variables by means of a multivariate optimisation with focus on geometry and topology related design aspects.

2 Electromagnetic Design

The HTS excitation generally allows for iron topologies that differ from conventional designs, i.e. the saving of heavy ferromagnetic parts for the guidance of magnetic flux [12]. The different topologies affect the magnetically effective air gap width and alter the magnetic design limitations due to iron saturation. Different iron topologies therefore imply differing electromagnetic utilisations and consequently differing main dimensions. Moreover, the presence of ferromagnetic parts next to the HTS tapes directly affects the current carrying capacity of the excitation winding and leads to operation conditions, in which different HTS tapes prove most suitable. The iron topology, the installation space and the HTS tape characteristics (with and w/o artificial pinning centres and at different operating temperatures) are thus interrelated. The covered scope of the analysis is described in the following subsections.

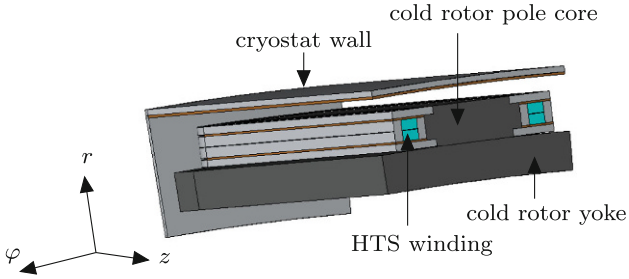

Fig. 1 Axial half of a rotor pole of a HTS DC excited direct-drive synchronous wind turbine generator with ferromagnetic rotor pole and rotor yoke (software: *JMAG Designer*)

2.1 Considered Iron Topologies

All considered direct-drive generators in this analysis are partially superconducting and feature a HTS DC excitation winding, Fig. 1, while the AC stator poly-phase winding conductors are made from copper. Superconducting AC windings have been considered in literature [11, 19, 23] and allow for an even higher electromagnetic utilisation but require an additional cryogenic cooling system, which increases the system complexity and the overall costs. In favour of a more robust design and reduced HTS material consumption, the analysis here is restricted to a superconducting DC excitation winding only. The considered iron topologies are shown as cross sections of one genera-

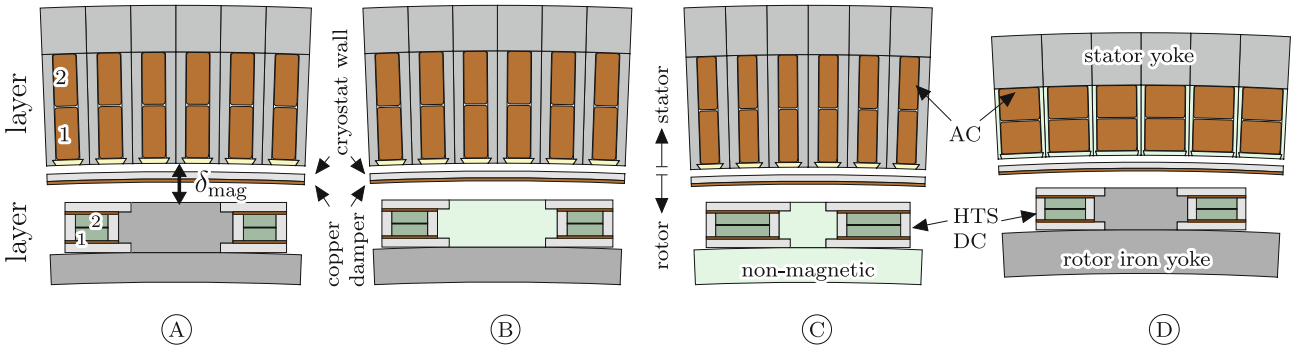

Fig. 2 Considered inner-rotor/outer-stator iron topologies per pole for the direct-drive HTS synchronous generator (for details see Sect. 2.1) with $q = 2$ slots per pole and phase for the stator poly-phase double-layer AC winding

tor pole in Fig. 2. Four topologies of the HTS generator are analysed:

A ferromagnetic stator yoke and teeth, ferromagnetic rotor pole and rotor yoke
B ferromagnetic stator yoke and teeth, non-magnetic rotor pole and ferromagnetic rotor yoke
C ferromagnetic stator yoke and teeth, non-magnetic rotor pole and yoke
D ferromagnetic stator yoke, ferromagnetic rotor pole and rotor yoke, stator air gap winding with non-magnetic support structure

The ferromagnetic stator yoke and the stator teeth for topologies A–C are made from laminated electrical steel M470-65A ($\gamma = 7700\,\mathrm{kg/m^3}$, [26]), while ferromagnetic massive rotor parts are made from FeNi9 ($\gamma = 8000\,\mathrm{kg/m^3}$, [22]). The non-linear $B(H)$-relations are shown in Fig. 8. Non-magnetic rotor parts and the non-magnetic support structure of the stator air gap winding in topology D are made from glass fiber reinforced plastic G10CR ($\gamma = 1850\,\mathrm{kg/m^3}$). The required rotor DC Ampere-turns per pole θ_f increase from topology A to C, while in case of D θ_f depends on the height of the stator air gap winding and hence on the stator current loading A_s.

All generator designs employ a single cryostat, which surrounds the cold rotor. The cryostat wall is made from non-magnetic stainless steel and contributes to the magnetic air gap width. A copper damper shield with thickness $d_\mathrm{Cu} = 5\,\mathrm{mm}$ ensures sufficiently low additional losses in the cold parts in spite of considerable air gap field harmonics due to slotting (topologies A–C), stator field harmonics and current harmonics due to inverter supply (all topologies). The damper is also used in presence of a stator air gap winding in order to provide sufficient screening of the HTS winding during transients (e.g. sudden short circuits, which yield high AC loss [28]). The thermal insulation is established by the vacuum, surrounding the cold parts, and by a multi-layer super-insulation, where the consumed space contributes to the magnetic air gap width ($\delta_\mathrm{mag} \approx 35\ldots40\,\mathrm{mm}$ for topology A). The HTS DC excitation windings are modelled as racetrack coils with either two layers (double racetrack coils, $n_\mathrm{Lf} = 2$, Fig. 2) or single layer racetrack coils ($n_\mathrm{Lf} = 1$, not shown). The restricted space in the pole gap for the excitation winding limits the use of single-layer excitation windings to topologies with low excitation requirements (e.g. Fig. 2A) or to low HTS operating temperatures to ensure higher critical currents I_c. The stator AC poly-phase winding in slots (Fig. 2A–C) is a $m = 3$ phase two-layer winding, which features $q = 2$ slots per pole and phase and a coil pitching by $W/\tau_\mathrm{p} = 5/6$ to reduce the 5th and 7th field harmonics. The stator air gap winding (Fig. 2D) is modelled as two-layer winding with $q = 2$ and the coil span W equal to the pole pitch τ_p in favour of a simpler end winding section without excessive width of the coil strands. This avoids a complicated bending of the end winding bar sections (in several planes), which would be necessary for a diametral, distributed single-layer winding in order to avoid crossing points. Due to the narrow support structure, only little difference regarding the current loading is however expected compared to a single layer air gap winding with $q = 1$.

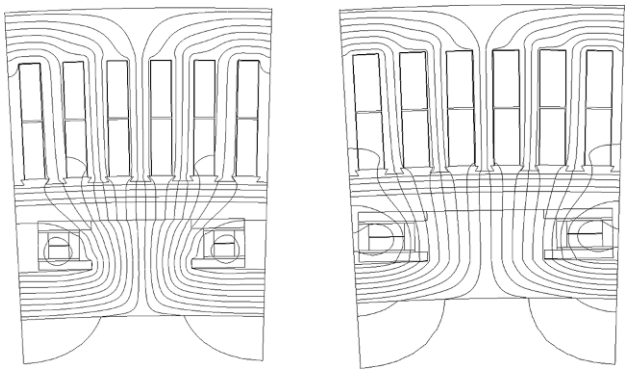

Fig. 3 Calculated magnetic field lines at no-load for an exemplary generator with all-iron topology A (Fig. 2) on the *left* and non-magnetic pole core B on the *right*

2.2 Design Procedure and Restrictions

The electromagnetic design is based on non-linear models employing the finite element method (FEM) with the free software *FEMM* [15], Fig. 3. Series of magnetostatic simulations are performed without consideration of eddy currents in order to save computation time. Previous analyses showed that the eddy current losses, particularly in the cold conductive parts, are low for the considered stator windings/damper dimensions and that the influence of the eddy current reaction on the magnetic field conditions is negligible at the very low stator frequencies ($f_\mathrm{s} \approx 5\ldots10\,\mathrm{Hz}$) [9]. The results obtained by magnetostatic simulations are validated against time-stepping transient 2D and 3D FEM simulations at load and no-load conditions implemented in the commercial software *JMAG*.

All models (*FEMM*, *JMAG*) feature a manually adjusted mesh with ~ 10^5 elements in case of 2D models. The number of nodes of the 3D models is in the order of $3.5\ldots4 \times 10^6$, Fig. 4. The models reported in this work solve for the magnetic vector potential A in the entire domain, since the superconductors' non-linear E–J-relation is not explicitly modelled. The computation of the AC loss by means of the H–A-formulation for selected designs revealed that the AC loss due to field harmonics are very small at stationary operation and are therefore not considered here.

The influence of stator current harmonics due to inverter supply is neglected here, while the stator inductances, even though generally large, are expected to vary among the topologies by yielding a different content of current harmonics. The high excitation

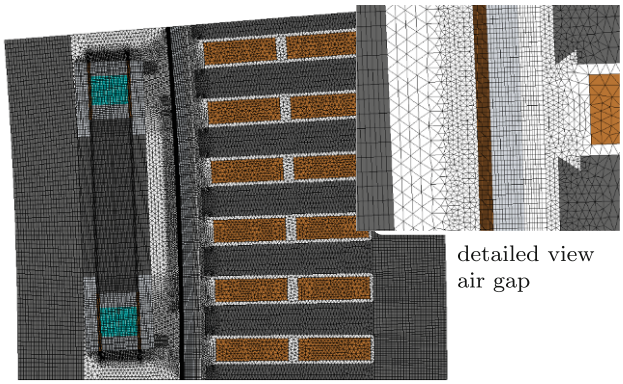

Fig. 4 Mesh of the transient, non-linear 2D generator model of one pole; detailed view of the air gap mesh

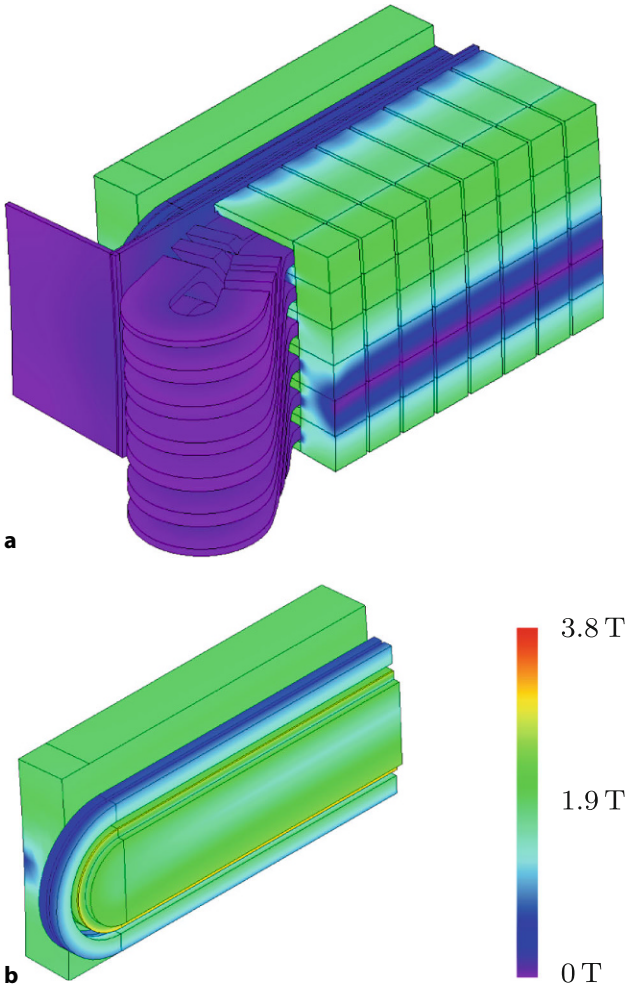

Fig. 5 Colour encoded, calculated magnetic flux density B at rated load for an exemplary generator with all-iron topology A (Fig. 2) **a** Axial half of one pole including stator and rotor, **b** detailed view of one axial half of one rotor pole with HTS excitation winding (software: *JMAG Designer)*

Table 1 Fixed generator specifications for all designs

Electric rated power $P_{\mathrm{el,N}}$	7 MW
Rated stator line-to-line voltage U_{N}	690 V
Rated speed n_{N}	8.33 rpm
HTS operating temperature T_{HTS}	20, 25, 30 K (see Sect. 2.3)
Circumscribing generator volume $V_{\mathrm{g}} = (\pi/4) \cdot d_{\mathrm{so}}^2 \cdot L$ (see Fig. 6)	25, 30, 35, 40 m^3
Operating strategy	MTPA

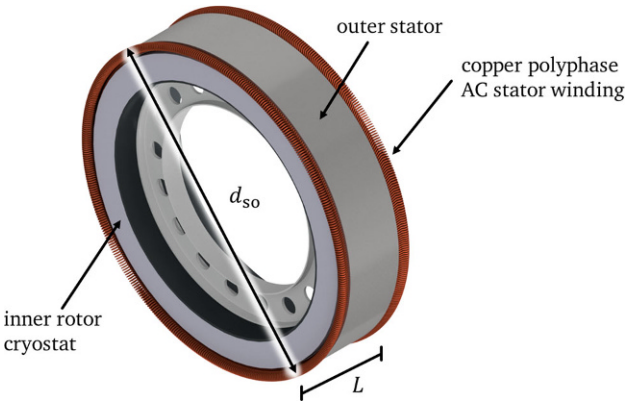

Fig. 6 Exemplary model of a HTS excited direct-drive synchronous generator with main dimensions that are scaled by the slimness λ_{d}, based on a prescribed circumscribing volume V_{g} according to Tab. 1 (software: *Autodesk Inventor*)

Ampere-turns θ_{f} generally lead to high flux densities, so that the iron saturation characteristic of the ferromagnetic materials, Fig. 8, plays a key role regarding the excitation requirements and the I_{c}-limiting flux density in the excitation winding „window“, i.e. the inter pole gap area. The fixed parameters are listed in Tab. 1, where the low voltage winding implies a large stator current and the use of several converters operated in parallel. The maximum torque per ampere (MTPA) operating strategy yields savings of the costly HTS material compared to $|\cos\varphi_{\mathrm{s}}| = 1$.

The geometry, including the pole count $2p$ and the number of layers of the excitation winding n_{Lf} (and hence the height of the rotor pole cores), are parametrised by eight non-dimensional variables $f_1 = \lambda_{\mathrm{d}}, f_2, \ldots, f_8$ [10]. First, the main dimensions are determined from the volume V_{g} by the „slimness“ $\lambda_{\mathrm{d}} = L/d_{\mathrm{so}}$, Fig. 6. The prescribed value of V_{g} plays a key role, as it determines the electromagnetic utilisation $C_{\mathrm{e}} = \text{torque/active volume} \sim A_{\mathrm{s}} \cdot B_{\delta 1} \sim S/(n_{\mathrm{N}} \cdot V_{\mathrm{g}})$ and the saturation state of ferromagnetic parts consequently ($B_{\delta 1}$: fundamental radial air gap flux density, S: apparent power). The choice of the considered volumes corresponds to *Esson*'s numbers [4] in the range $C_{\mathrm{e}} \approx 18\ldots29\,\mathrm{kVA \cdot min/m^3}$.

Based on these fixed quantities and the eight non-dimensional variables f_{i}, the HTS synchronous generators are designed by an automated, iterative procedure, which adjusts the lead angle γ, the electrical

Table 2 Non-dimension variables of parametric model

λ_d	Axial length L / stator outer diameter $2r_\mathrm{so}$
f_p	Scaling factor: no. of pole pairs in the range $p = 20\ldots80$
f_Lf	Scaling factor: no. of layers of excitation winding
$f_\mathrm{ri,ro}$	Rotor inner radius r_ri / stator outer radius r_so
$f_\mathrm{\delta,\Delta r}$	Ratio radial dimension of rotor ($\overline{r}_\delta - r_\mathrm{ri}$)/ radial dimension of rotor and stator ($\overline{r}_\delta$: radius in the middle of the geometric air gap)
f_ys	Ratio stator yoke height h_ys / radial dimension of stator core ($r_\mathrm{so} - r_\mathrm{si}$)
$f_\mathrm{b,\tau,Q}$	Ratio slot width (arc length) s'_Q / slot pitch (Q: stator number of slots; s_Q: slot width)
$f_\mathrm{w,\tau,p}$	Ratio width of pole core (arc length) w'_p / pole pitch (w_p: width of pole core)

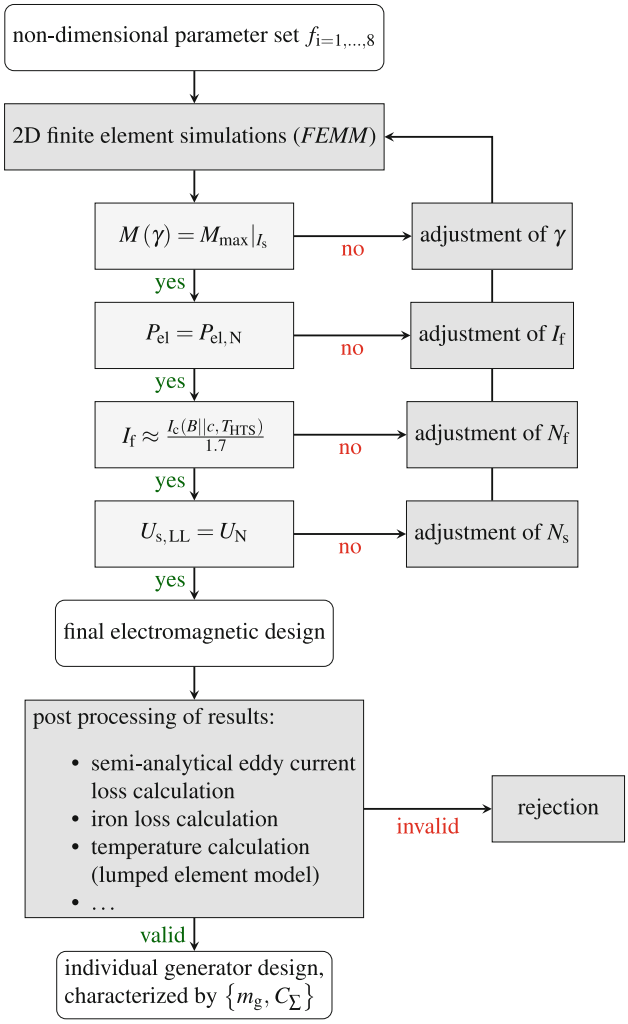

Fig. 7 Simplified flowchart of the design procedure, $B||c$ denotes the magnetic flux density in the excitation winding window with the most critical orientation parallel to the tape's c-axis

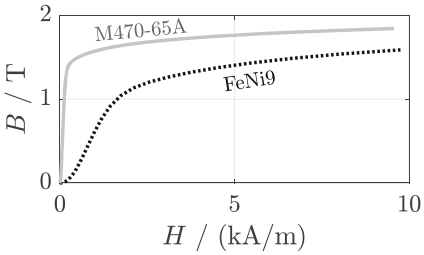

Fig. 8 $B(H)$-characteristics for the considered ferromagnetic materials: cold rotor parts made from FeNi9, stator iron stack made from M470-65A electrical steel [22, 26]

output power P_el, the number of turns of the excitation winding $N_\mathrm{f} = 2p \cdot N_\mathrm{f,pole} = 2p \cdot \theta_\mathrm{f}/I_\mathrm{f}$ and the stator line-to-line voltage U_s to the prescribed values, Fig. 7. The critical current of the HTS winding I_c is determined for each FEM simulation run, based on the most critical operating conditions, determined by the absolute value and orientation of the flux density $\vec{B}$ in the winding window (at a given operating temperature T). A margin of $I_\mathrm{f}/I_\mathrm{c} = 1/1.7$ is kept in order to ensure stability with respect to electrical and thermal transients. Based on the DC excitation current I_f the number of turns $N_\mathrm{f}/(2p) = \theta_\mathrm{f}/I_\mathrm{f}$ is adjusted, while the restriction of the available space in the rotor pole gap is incorporated.

Details of the iterative design procedure as well as of the thermal model, which is used to estimate the required cryogenic cooling capacity, are described in [10], which covers however only the all-iron topology for a single tape and cryogenic temperature. In spite of the much larger variability of the compared variants in this work, the current density in the copper stator winding is always $J_\mathrm{Cu} = 3.8\,\mathrm{A/mm^2}$ and the copper filling factor in the winding window of the slots is $k_\mathrm{Cu} = 0.75$ due to the use of profile copper and a low voltage $< 1\,\mathrm{kV}$. The evaluation of individual designs' efficiency incorporates the *Ohmic* loss in the stator winding, the iron loss in rotor and stator, the eddy current loss in the cryostat wall and the damper and the compressor input power of the cryogenic cooling system. Mechanical losses are not considered because they are generally small due to the very low rotational speed, particularly compared to the *Ohmic* loss in the stator winding.

2.3 HTS Tape Characteristics

Two rare-earth barium copper oxide (ReBCO) tapes with a tape width of $w_\mathrm{t} = 12\,\mathrm{mm}$ are considered since this material class proves advantageous regarding low m_g, V_g compared to MgB_2 wires [16]. The tapes differ with respect to the presence of artificial pinning centres, yielding different lift factors at low temperatures and moderate external magnetic fields, Fig. 9. Three cryogenic operating temperatures of the HTS excitation windings are considered, $T = 20, 25, 30\,\mathrm{K}$. The large margin with respect to

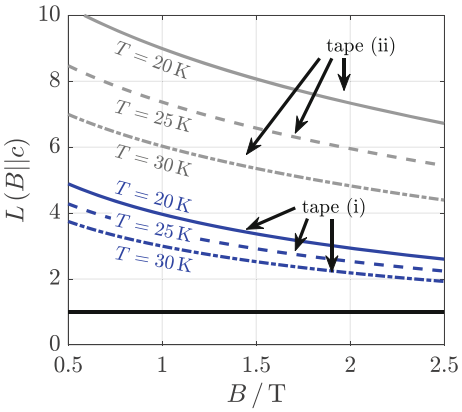

Fig. 9 Lift factor $L = I_c / I_c\,(77\,\mathrm{K}$, self field) of the critical current in case of HTS tapes (i) and (ii) as a function of the external field $B||c$ for the considered operating temperatures T, fits to manufacturer data from [5, 24]

the jump temperature $T_c \approx 90\,\mathrm{K}$ allows for lift factors $L = I_c\,(T, \vec{B}) / I_c\,(77\,\mathrm{K}, 0\,\mathrm{T}) \geq 2$ and therefore for a good utilisation of the costly HTS material. The lift factors are derived as fits to manufacturer data, where this kind of tapes can be purchased from several manufactures, e.g. *THEVA* or *Fujikura*.

Tape (i) does not feature artificial pinning centres (APCs) and has consequently a smaller in-field lift factor at low temperatures than tape (ii) with APCs. Tape (ii) is therefore considered to be the better choice in case of topologies with less ferromagnetic parts, where higher flux densities $B \geq 2\,\mathrm{T}$ occur in the excitation winding and where higher ampere turns θ_f must be provided for the same space in the inter pole gaps (e.g. for topologies C and D). In contrast, tape (i) is mainly suitable if the flux is guided by iron parts, such as topology A, where the flux density is in the range of $B \approx 1.5 \ldots 1.7\,\mathrm{T}$ and if cost advantages are considered, Sect. 4.

2.4 Evaluation of Individual Designs

The considered HTS synchronous generator designs are generated during a numerical optimisation by means of a genetic algorithm (GA), separately for each of the topologies A…D and for each set of constraints,

Table 3 Specific prices assumed for material and components, based on information provided by companies [2, 5, 8, 20, 24, 27]

HTS tape (i) (77 K, self field)	100 €/(kAm)
HTS tape (ii) (77 K, self field)	250 €/(kAm)
AC/AC inverter	30 €/kVA
Cooling system per cold head	25000 €
Copper for stator winding	13.5 €/kg
Stainless steel	3 €/kg
Steel sheets	3 €/kg
FeNi9 ferromagnetic steel	3 €/kg
G10CR glass fibre compound	15 €/kg

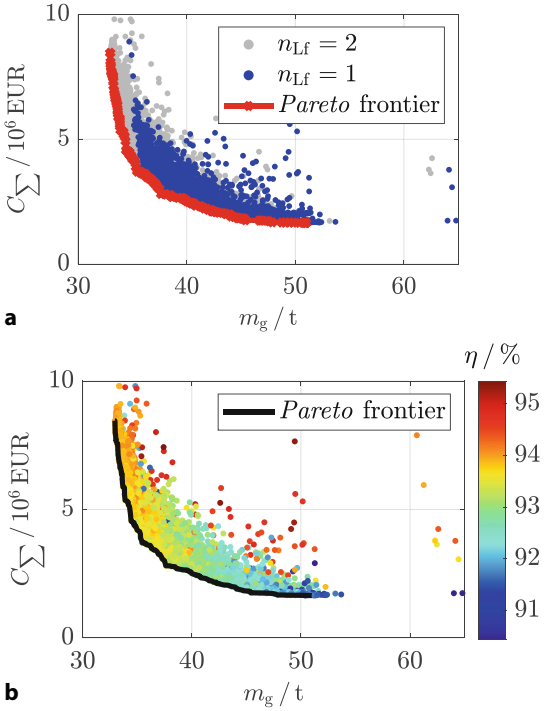

Fig. 10 7 MW synchronous generators, 8.33 rpm, 690 V: Calculated *Pareto* frontier for generator topology A (Fig. 2) in a plot of total cost versus active generator mass together with the entire set of simulated individuals: **a** colour encoded number of layers of the excitation winding $n_{Lf} = 1$ or 2, **b** colour encoded generator efficiency η

Sect. 2.2. The eight non-dimensional parameters f_i represent the optimisation variables, while the system costs C_Σ and the active generator mass m_g (excluding inactive parts like frame structures) serve as competing objectives. The pre-implemented GA of the commercial software *MATLAB* is used with parameters ParetoFraction=0.35 and CrossoverFraction=0.8. The optimisations are run on 48 cores with a clock rate of 3 GHz.

C_Σ in (1) is chosen to comprise the main design sensitive cost contributions: generator material cost including the HTS material, cost of the full inverter system, which is depending on the rated apparent power S and hence on the power factor $\cos\varphi_s$ and the cost of the cryogenic cooling system. Specific prices are listed in Tab. 3.

$$C_\Sigma = C_{\text{gen., material}} + C_{\text{inverter}} + C_{\text{cryo cooling}} \tag{1}$$

An exemplary visualisation of an entire set of HTS generator designs together with the *Pareto* frontier of C_Σ versus m_g is shown in Fig. 10a, where the two choices for the number of layers of the HTS excitation winding are colour encoded. Heavier generator designs are suitably excited with single-racetrack HTS coils by reducing the rotor inter pole stray flux and the length of the main flux path. However, lightweight designs require two layers $n_{Lf} = 2$ in order to provide the increased required ampere turns per pole θ_f. In

the following, only *Pareto* efficient individuals (with respect to $\{C_\Sigma, m_g\}$) are considered for different basic conditions and topologies, since these objectives are considered to be paramount. This narrows the scope to generator designs that are generally not efficient regarding other considered key quantities. This can for example be observed in case of the overall generator efficiency, Fig. 10b, where highest values of $\eta \approx 95\%$ are featured by individuals that are not part of the *Pareto* frontier. The large variation of the active mass in the range $m_g = 35\ldots55\,\mathrm{t}$ for fixed V_g is attributed to the very high excitation ampere turns Θ_f, which enables minimum iron mass (i.e. reduced yoke heights) at the cost of excessive HTS material consumption.

3 Performance at Rated Operation

The GA optimisation runs yield for topologies A...D sets of 25000...40000 individual HTS generator designs, for which only the *Pareto* efficient ones are discussed in the following subsections. For each topology and set of fixed parameters, a sufficient exploration of the eight-dimensional design space $f_i\, i = 1, \ldots, 8$ is ensured by inspection of the covered variable ranges. The generator designs are evaluated for a single rated operating point 7 MW, 8.33 rpm, 690 V according to Sect. 2.2.

3.1 Comparison of Iron Topologies

The considered topologies A–C, Fig. 2, are compared for the same circumscribing volume $V_g = 40\,\mathrm{m}^3$, the same cryogenic operating temperature $T = 30\,\mathrm{K}$ of tape (i) and a maximum stator outer diameter of $d_{so}^{max} = 6.515\,\mathrm{m}$. In case D with stator air gap winding, yielding an increased stator current loading A_s, a smaller volume $V_g = 25\,\mathrm{m}^3$, but also $d_{so}^{max} = 6.515\,\mathrm{m}$ and a lower operating temperature $T = 20\,\mathrm{K}$ are considered. The HTS generators with topology D feature an excitation winding made from tape (ii) to utilize its better in-field performance.

In all four cases, the required total HTS tape length l_{Tape} increases with decreasing generator active mass since the heavy iron parts with large cross section reduce the required excitation ampere turns θ_f. The comparison between topologies A–C, which use tape (i), shows that topology A with ferromagnetic pole core and rotor yoke dominates those generator designs (B and C), where the rotor is entirely or partially non-magnetic, Fig. 11a. The mass reduction due to the lighter composite material comes at the cost of a disproportionate increase in the required HTS material amount. This result is consistent with [6]. The limited space in the rotor inter pole gap moreover restricts geometrically the design options for the topologies B and C with less ferromagnetic parts. The lack of flux guidance in case of a non-magnetic rotor structure B, C increases the rotor inter pole stray flux, which additional loads the rotor iron yokes magnetically. The rotor yoke heights must accordingly be increased in order to achieve the demanded power. The HTS generators D with stator air gap winding dominate the other designs A, B, C with slotted stator, regarding reduced active mass at similar total HTS tape length for following reasons:

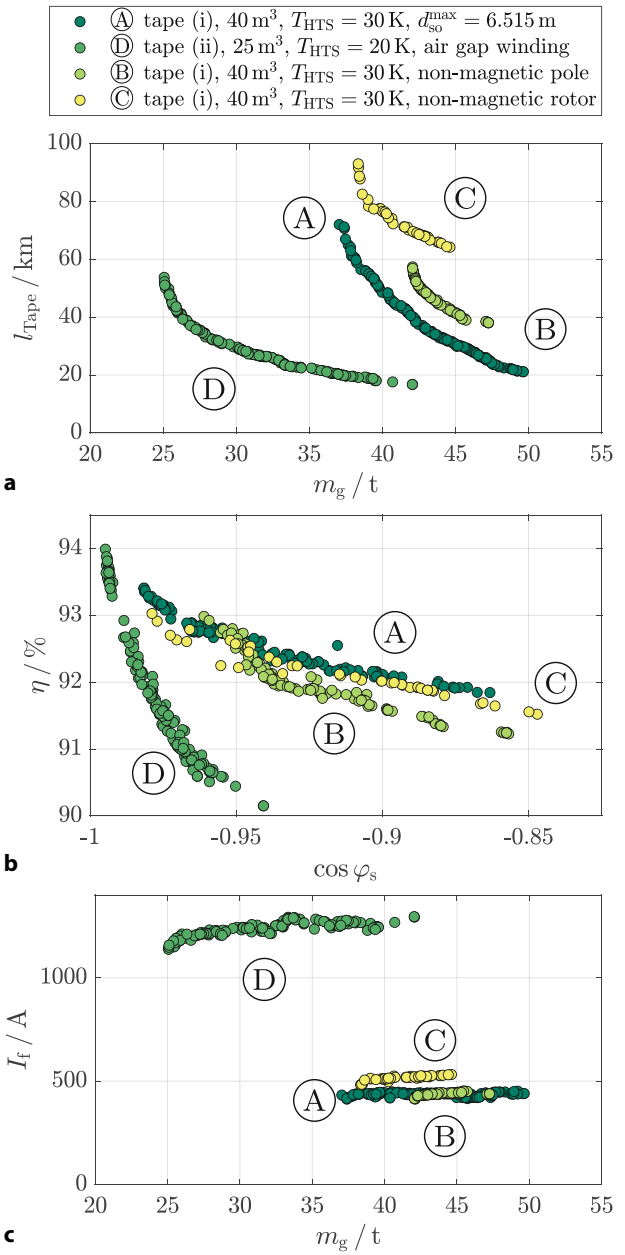

Fig. 11 Calculated results, variants A–D (Fig. 2): **a** total length of required HTS tapes for all rotor poles vs. generator active mass, **b** overall generator efficiency versus rated power factor, which is here negative in the consumer reference frame, **c** superconducting excitation current I_f at rated operation 7 MW, 8.33 rpm, 690 V

1. The reduced circumscribing volume in case D accounts for the increased electromagnetic utilisation $C_e \sim A_s$ and implies a reduced mass of all active parts. Previous studies revealed, that the stator

air gap winding only provides benefits, if a more compact design accounts for the increased current loading A_s at a comparable magnitude of the air gap field fundamental $B_{\delta 1}$.

2. Tape (ii) has a higher in-field critical current I_c allowing for considerably higher excitation currents I_f (Fig. 11c), particularly at the reduced operating temperature $T = 20\,\mathrm{K}$. This choice also anticipates the increased excitation demand θ_f due to the air gap winding. The reduced amount of required HTS material does not necessarily translate to reduced material costs, since tape (ii) has a higher price per unit length, Sect. 4.

The rated power factor $\cos\varphi_s$ is comparably high for each of the considered topologies A…D, Fig. 11b, which is attributed to the high rotor field and the inductance-limiting effect of the large magnetic air gap width δ_{mag}, Fig. 2. Designs with low HTS material consumption feature the lowest absolute values $|\cos\varphi_s| \approx 0.85$. Most efficient designs are enabled by a high rotor field and are therefore also characterised by $|\cos\varphi_s| > 0.975$, so that high efficiency and high power factor go hand in hand. The comparison of topologies A–C reveals advantages of highly magnetically utilised all-iron designs, while similar results are found for an entirely non-magnetic rotor structure C. Topology B with non-magnetic pole core turns out to be disadvantageous regarding η and $\cos\varphi_s$. The HTS design D with stator air gap winding outperforms the alternatives with slotted stator in case of highest electromagnetic utilisation (consistent with [17]), whereas the overall efficiency suffers from the larger stator current loading A_s due to the reduced rotor field amplitude $B_{\delta,1}$. This result is consistent with [14].

A higher rotor inter pole stray flux $\Phi_{p\sigma}$ generally reduces the critical current I_c and in this connection further increases l_{Tape}. For the comparison of the topologies A…C with slotted stator and similar C_e, the smallest I_c-reduction is observed for an entirely non-magnetic rotor structure C due to the absence of low-reluctance stray paths, Fig. 11c. The difference in the field dependent lift factor L between non-magnetic (B) and ferromagnetic pole cores (A) is not significant, because the iron rotor yoke permeability mainly determines the field conditions at the HTS coil's position.

The comparison of the pole count $2p$ of the *Pareto* efficient individuals, Fig. 12a, reveals only small differences between the topologies A…C with slotted stator. For topologies B and C with non-magnetic rotor parts all efficient generator designs feature an identical pole count, i.e. $2p = 74$ and $2p = 76$. Larger pole counts would reduce the required yoke heights, but come at the cost of additional HTS material and are for high values of $2p$ excluded due to the limited space in the inter pole gaps. Efficient designs with topology D with stator air gap winding are characterised by considerably smaller pole counts $2p = 52…70$, which

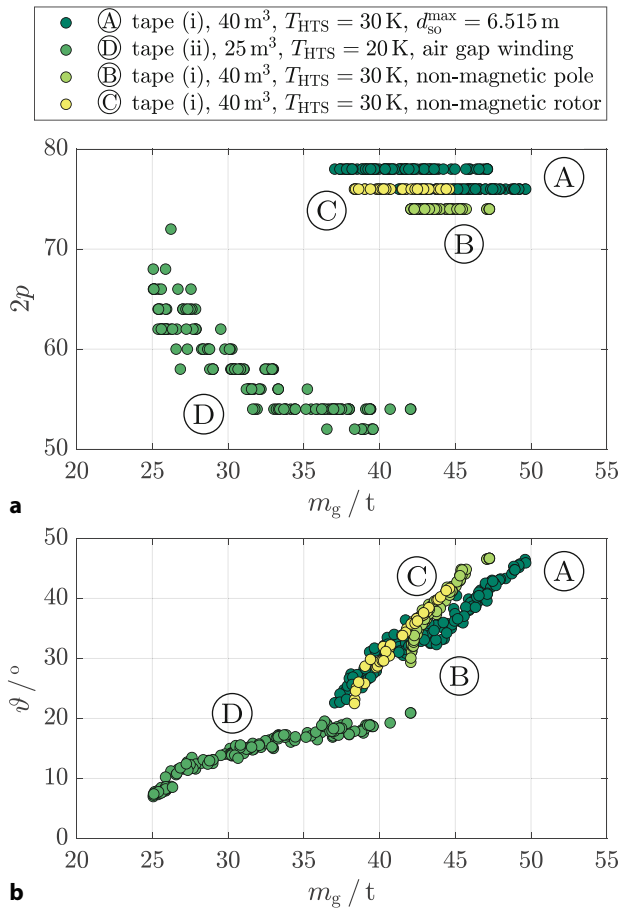

Fig. 12 As Fig. 11, but: **a** pole count $2p$, **b** load angle ϑ in electrical degrees at rated operation versus generator active mass

even decrease towards heavier designs with larger iron cross sections. This result is attributed to the requirement that the ratio between magnetic air gap width and pole pitch δ_{mag}/τ_p must not become too large in order to obtain sufficient torque producing main flux linkage.

The different magnetic conditions for topologies A…D also manifest in different load angles ϑ at rated operation, Fig. 12b. As can be expected, more lightweight designs yield lower stator winding inductances L_d, L_q that imply a lower load angle. The rated operating points differ only little in this regard among the designs A…C with slotted stator, since the magnetic environment of the stator winding is similar and the influence of the magnetic conditions in the rotor on the stator inductances L_d, L_q is rahter small.

The more compact generator design D with the stator air gap winding exhibits however considerably smaller inductances L_d, L_q and load angles ϑ because of the slot stray inductance, which is of influence in case of the slotted windings due to the large slot height h_Q, see Fig. 2, but is strongly reduced in case of the air gap winding. The smaller the values of L_d, L_q among the considered designs A…D, the less they can limit

the stator current harmonics due to inverter feeding, which is however not part of this study.

3.2 Influence of Installation Space and Outer Diameter

Besides the choice of the topology A…D, the generators' main dimensions determine the electromagnetic utilisation C_e and hence the magnetic conditions inside the generator. The installation space in the nacelle usually restricts the maximum outer diameter d_{so}. Small circumscribing volumes V_g are an advantage that is supported by the HTS DC excitation. Smaller values of V_g do however not necessarily yield more lightweight generators, so that this section compares *Pareto* efficient generator designs with topology A (all iron, minimum amount of HTS material required) for different main dimension limits. Two optimisation runs with the same tape (i), the same volume $V_g = 40\,m^3$ and the same cryogenic operating temperature $T = 30\,K$ are considered for two cases:

1. $d_{so}^{max} = 6.515\,m$: The stator outer diameter is restricted according to typical dimensions of commercially available wind generators with $P = 7\,MW$ power rating [21].
2. d_{so} not restricted: For fixed volume V_g, the diameter is essentially restricted by a disproportionate increase of the stator and rotor end winding length. In case of the stator, this causes corresponding ohmic losses. For the stator winding Thermal Class F (IEC 60034-1) is assumed with $\Delta\vartheta = 105\,K$ temperature rise over 40°C ambient. The limit is checked by means of the thermal model. This scenario is considered in order to assess the impact of the restricted diameter d_{so} for HTS excited generators.

In addition, two optimisation runs for topology A with the same maximum outer diameter $d_{so}^{max} = 6.515\,m$, but reduced circumscribing volume V_g are considered. Even though the stator outer diameter can generally differ from its maximum value due to the scaling with the slimness factor λ_d, all *Pareto* efficient individuals feature approximately $d_{so} = d_{so}^{max}$, as expected from the approximate scaling of the torque $M \sim d_{so}^2 \cdot L$.

The minimum generator active mass is obtained for HTS generator designs without upper limit on the outer diameter, Fig. 13a. This finding is attributed to the much higher pole counts $2p = 110…140$ compared to $2p = 70…80$ in case of a restricted outer diameter d_{so}^{max}. The yoke heights are accordingly reduced to about 60% of the value with smaller diameter, so that the yokes' significant contribution to the generator's active mass is smaller. In order to achieve the same active mass with smaller stator outer diameter d_{so}^{max}, an about 3 times higher amount of HTS material is required, as iron saturation sets in for a higher flux per pole Φ_p and similar yoke heights. The worse flux guidance moreover leads to an I_c-reduction, as the flux density in the excitation winding increases.

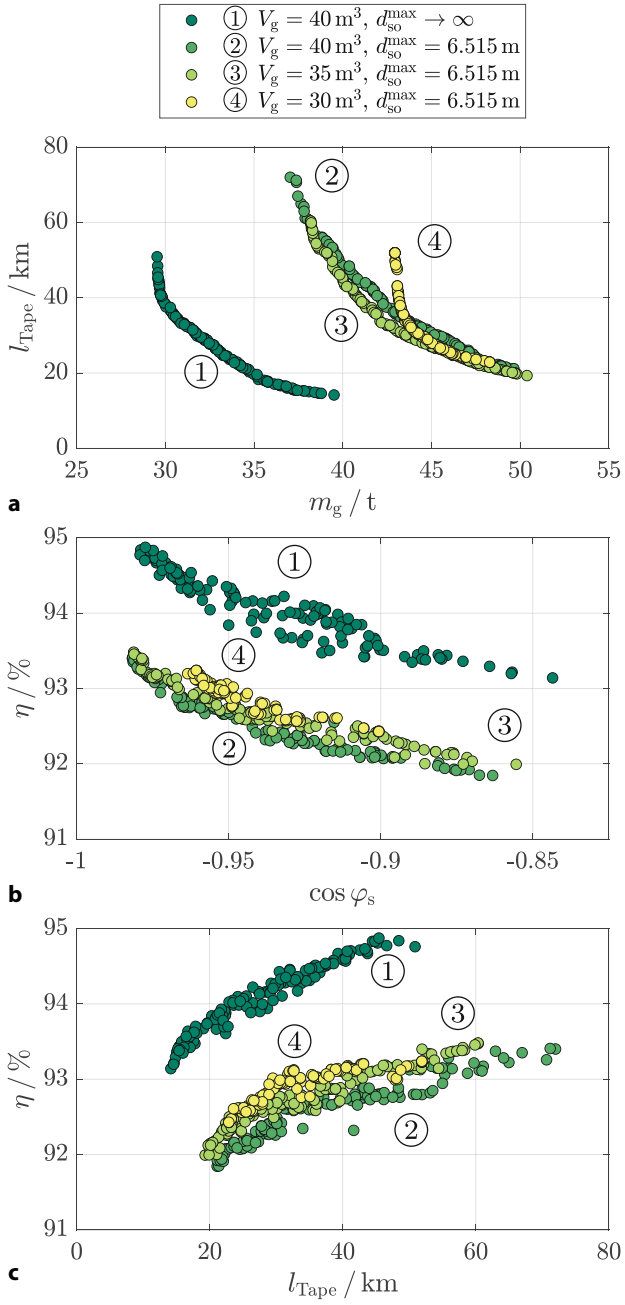

Fig. 13 Variation of V_g, $d_{so,\,max}$ for generator topology A, HTS tape (i), $T_{HTS} = 30\,K$ (Fig. 2): **a** total length of required HTS tapes of all rotor poles versus generator active mass m_g, **b** overall generator efficiency η versus rated power factor (negative in consumer reference frame), **c** generator efficiency vs. total HTS tape length

Compared to the case of a maximum outer diameter, the prescribed volume V_g has only little influence on the ratio between l_{Tape} and m_g, Fig. 13a. Opposing effects of a volume reduction are:

1. The reduced generator axial length L implies axially shorter poles with shorter tape lengths per pole. The shorter axial length directly reduces the size and the mass of active parts.

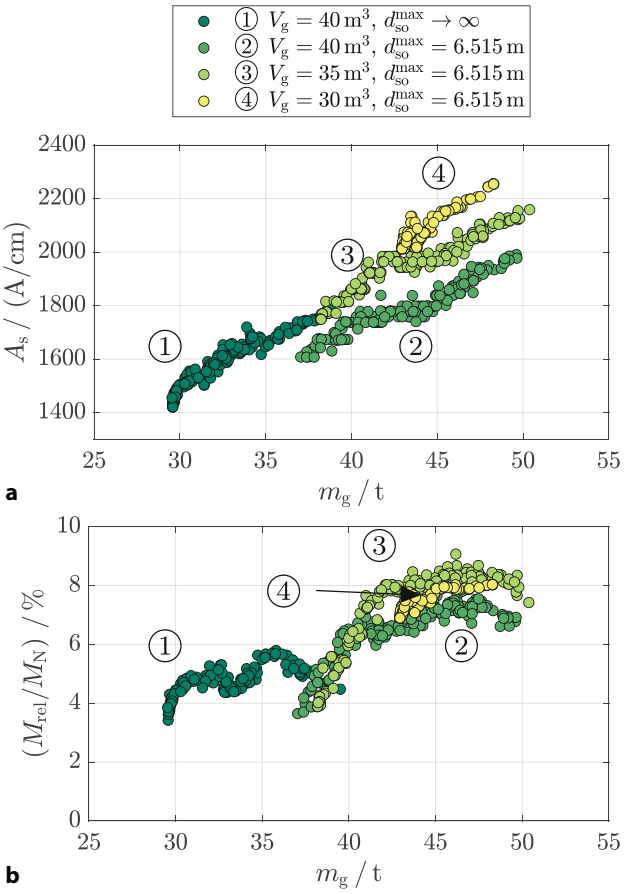

Fig. 14 As Fig. 13, but: **a** stator current loading versus generator active mass, **b** share of reluctance torque M_{rel} in the rated torque M_N versus generator active mass m_g

2. The torque producing air gap field must be increased by means of higher θ_f to achieve the higher electromagnetic utilisation $C_e \sim A_s \cdot B_{\delta 1} \sim 1/V_g$ for approximately fixed apparent power S and speed n, even if the stator current loading A_s is also increased to some extent, Fig. 14a. The higher air gap field requires larger yoke heights for flux guidance.

The comparison, Fig. 13a, reveals that these effects nearly cancel out so that a reduction of V_g has only limited potential to decrease the active mass and the HTS material consumption in the studied range.

Still, the shorter axial length L implies lower ohmic loss even if A_s is increased (Fig. 14a), which manifests in efficiency advantages towards smaller V_g, Fig. 13b and c since the stator ohmic loss dominates for low-speed direct-drive generators. For a given power factor, the larger stator outer diameter moreover proves advantageous in terms of a higher generator efficiency due to the reduced stator current loading. With a restricted outer diameter, it is the minimum circumscribing volume $V_g = 30\,m^3$ where the HTS tape is more effectively used for an increase of the generator efficiency, Fig. 13c.

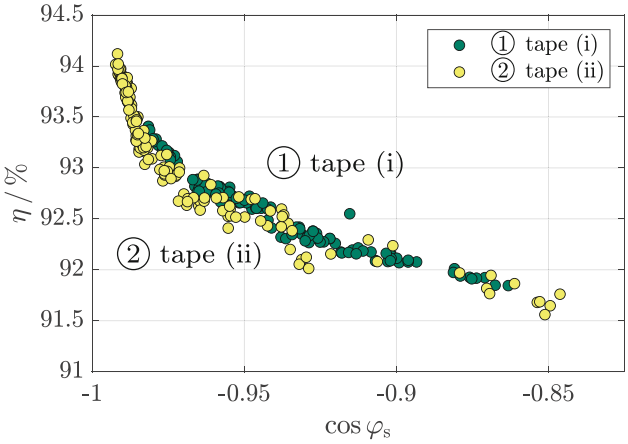

Fig. 15 From Tab. 1: $V_g = 40\,m^3$, $T_{HTS} = 30\,K$, $d_{so,max} = 6.515\,m$, generator topology A and excitation windings made from two different tapes (i) & (ii) (Sect. 2.3): Calculated generator overall efficiency versus rated power factor

In all considered cases 1…4, the high stator current loadings of *Pareto* efficient designs, Fig. 14a, are accompanied by a high thermal utilisation $\Delta\vartheta_{Cu} \sim A_s \cdot J_s$, which requires a powerful stator cooling system to limit $\Delta\vartheta_{Cu}$ to 105 K. This cooling concept should ideally lead to a thermal decoupling of the cold rotor and warm stator parts. Regardless of the considered installation space and the maximum diameter, the share of the reluctance torque in the overall rated torque for optimum generator designs with all-iron topology A is small, Fig. 14b: The reluctance torque always contributes less than 10% with decreasing share towards highly-saturated, lightweight variants.

3.3 Comparison of HTS Materials

The choice of the HTS tape and of the cryogenic operating temperature T determines the number of turns N_f and consequently the dimensions of the excitation winding window that are required to provide the necessary ampere turns θ_f. It moreover affects the inductance of the excitation winding L_f, which is however not analysed in this work. Tape (ii) has a higher critical current than tape (i) at a given temperature T and field B, which influences the electromagnetic design:

- With tape (ii), larger widths w_p of the pole cores are possible for the same excitation θ_f, which relieves one potential magnetic bottleneck of iron saturation.
- Higher flux densities in the excitation winding window are admissible due to the better in-field performance of tape (ii) so that a higher saturation of the rotor parts (particularly the rotor yoke) are tolerable.
- Higher fields for same space requirements in the inter pole gap allow for smaller current loadings A_s in order to obtain the same utilisation C_e.

There is no significant difference for tapes (i) & (ii) (Fig. 9) in case of generators of topology A with re-

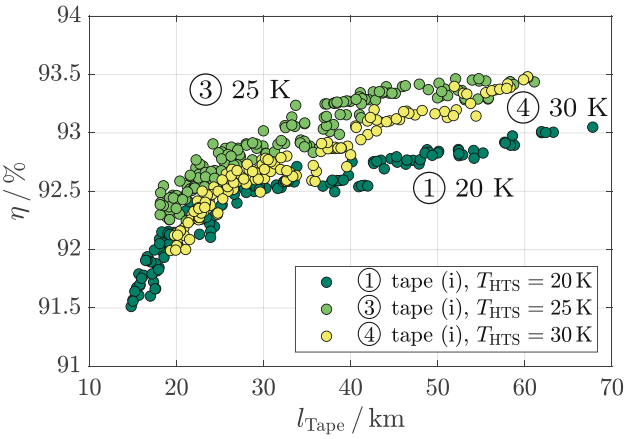

Fig. 16 As Fig. 15, but $V_g = 35\,m^3$, with different operating temperatures of the HTS excitation winding: Generator overall efficiency versus required tape length

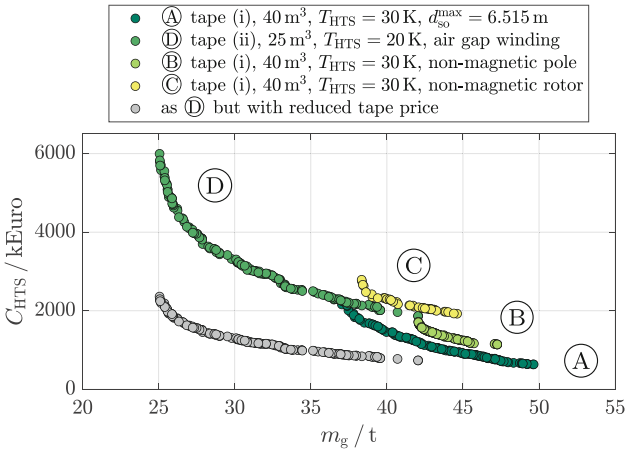

Fig. 17 Different iron topologies A…D according to Sect. 3.1: HTS tape cost at $n_{Lf} = 2$ versus generator active mass m_g

spect to generator efficiency η and power factor $\cos\varphi_s$, Fig. 15. For the given topology A, the power factor can be regarded as a measure for the saturation state whereas the efficiency is mainly determined by the stator current loading, as *Pareto* efficient designs almost always exhibit outer diameters $d_{so} = d_{so}^{max}$. Since the electromagnetic utilisation C_e is fixed by V_g, n_N and P_N, the designs are characterised by a trade-off between high rotor field (and thus saturated iron with higher power factor) and high current loading (and thus reduced efficiency). This relation turns out to be generic, while the tape with higher in-field performance allows to extend the achievable range towards even higher absolute values of the power factor and generator efficiencies.

The choice of the operating temperature T_{HTS} is characterised by the balance between

1. a good utilisation of the HTS tape material in terms of high admissible excitation currents I_f, Sect. 2.3, and
2. a manageable cryogenic cooling power, which determines the cooling system's cost and the influence on the efficiency.

The comparison between the *Pareto* efficient designs of optimisation runs that differ only with respect to the cryogenic operating temperature T_{HTS} reveal that a temperature of $T = 25\,K$ with an estimated coefficient of performance of the cryogenic cooling system: COP ≈ 1.1% is advantageous, Fig. 16. In this case, the reduction of the required amount of HTS material compared to $T = 30\,K$ is significant and the higher I_c-values allow for an increased rotor field and a reduction of the stator current loading. The latter effect overcompensates the moderate increase of the cooling power ($T = 30\,K$: COP ≈ 1.3%). A further reduction of the operating temperature to $T = 20\,K$ with COP ≈ 0.7% leads to a disproportionate increase of the cooling system's input power with accordingly lower overall generator efficiency.

4 Economic Considerations

Besides technical advantages of the HTS excitation compared to the alternative state-of-the-art PM excitation, regarding higher η and $|\cos\varphi_s|$, economic considerations are vital for a future commercialisation [13]. Generally, the strongly reduced dependence on rare earth (RE) materials is a major benefit of the HTS technology, since REs are subject to disposability risks. One approach to assess the economical feasibility is the consideration of the levelized cost of energy (LCoE) [1], which for example directly incorporates efficiency advantages, but requires several additional assumptions on dynamical variables, e.g. the feed-in remuneration. Therefore, this study considers the investment costs only by aiming to include all decision sensitive cost contributions, Sect. 2.4. Meaningful conclusions from the optimization results regarding economical competitiveness should therefore rely on comparisons of generator designs with equal efficiency. To date, the HTS production capacities are, even though increasing, still low, so that the HTS tape costs generally dominate the overall costs. As this cost share mainly consists in manufacturing costs, a cost decrease due to economies of scale is probable in the near future.

4.1 HTS Tape Cost

The amount of required HTS tape differs strongly for different magnetic topologies A…D, Sect. 3.1, and can be influenced by the cryogenic operating temperature T_{HTS}, Sect. 3.3. The advantages of all-iron designs A in case of a slotted stator are also apparent from the relation between HTS tape cost and the generator active mass, Fig. 17. Irrespective of the HTS tape price, the tape is most effectively used for topology A in order to achieve the minimum weight. Still, the cost share of the HTS tape in the overall material cost is in the range of 55…65% for *Pareto* efficient designs.

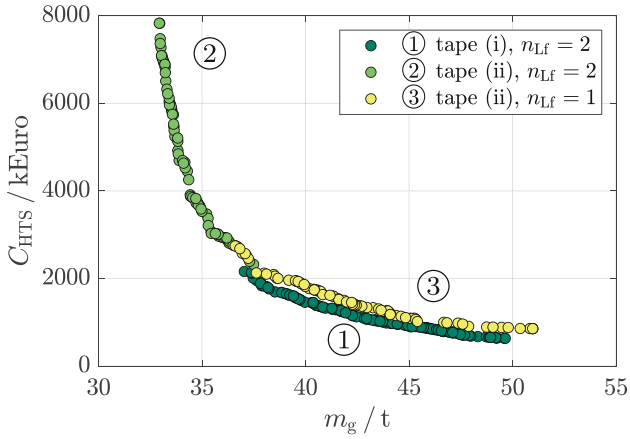

Fig. 18 From Tab. 1: $V_g = 40\,m^3$, $T_{HTS} = 30\,K$, $d_{so,max} = 6.515\,m$ with different HTS materials according to Sect. 3.3 (with either $n_{Lf} = 1$ or $n_{Lf} = 2$ layers of the excitation winding): Calculated HTS tape cost versus generator active mass

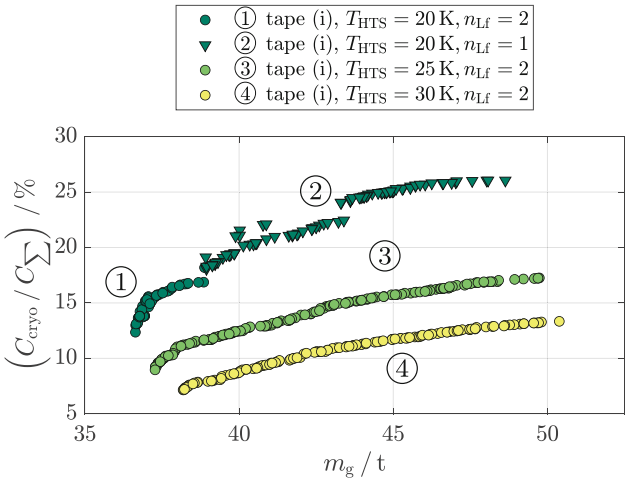

Fig. 19 As Fig. 18, but $V_g = 35\,m^3$, HTS tape (i), with different cryogenic operating temperature 20, 25, 30 K of the HTS winding: Calculated cost share of the cryogenic cooling system versus generator active mass

The comparison with the design D featuring the stator air gap winding, Fig. 17, reveals that the higher price for tape (ii) outweighs the smaller amount of required tape (Fig. 11a), while the lower operating temperature T_{HTS} implies a more costly cooling system. To date, the current carrying capacity related prices therefore promote topology A as the most economic solution. Current developments [25] give however rise to the expectation that improved tapes with APCs (like tape (ii)) could be available at the present price of tape (i) ($p' = 100\,€/kAm$) in the near future. Fig. 17 therefore also shows the *Pareto* efficient individuals for this scenario in light grey (topology D). In this case, very compact ($V_g = 25\,m^3$) and lightweight HTS generator designs with a stator air gap winding would be competitive and commercially viable, even without consideration of technical advantages in terms of high efficiency and power factor, Fig. 11b.

For the current price difference between the tapes, the higher performance of tape (ii) is however overcompensated by the disproportionally higher price in case of the all-iron topology A, Fig. 18. This allows the conclusion that tape (ii) is currently only a reasonable alternative if the goals of reduced volume and mass are paramount. For several sets of fixed conditions (particularly $T = 30\,K$), it is moreover only tape (ii) that enables an excitation winding with only one layer $n_{Lf} = 1$. This allows for a favourably shorter main flux path and a slightly reduced rotor inter pole stray flux $\Phi_{p\sigma}$.

4.2 Cost Share of Inverter and Cryogenic Cooling System

The inverter rating is directly determined by the electromagnetic design via the power factor $\cos\varphi_s$ at a fixed electric output power P. The generator geometry with its warm and cold surface areas and dimensions of mechanical supports, and the varied cryogenic operating temperature T_{HTS} affect the cost of the cryogenic cooling system. The comparison of this share in the system cost, Fig. 19, shows a minor contribution < 15% for $T = 30\,K$. More lightweight generators generally imply higher HTS material costs, while the cooling system's cost remains nearly the same. In case of lower operating temperatures, the

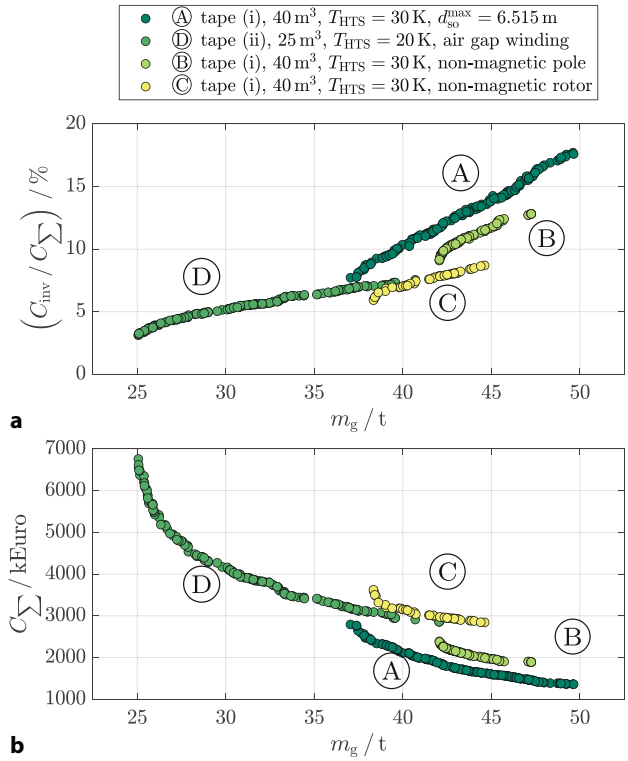

Fig. 20 Different iron topologies A–D (Fig. 2) according to Sect. 3.1: **a** cost share of the full inverter system in the system cost, **b** system cost versus generator active mass

share of the cryogenic cooling system reaches up to 25%, which is in the range of the HTS material cost. The stronger decrease of the cooling system's share towards low generator masses $m_g < 40\,t$ implies that lower operating temperatures $T < 25\,K$ are mainly suitable, if high saturated lightweight generator designs are considered in order to limit the disproportionate increase of required HTS material.

The comparison of the cost share of the full inverter system for topologies A-D, Fig. 20a, reveals its minor role in case D of HTS generators with stator air gap winding. This finding is attributed to the high power factor, and thus low inverter rating, and to the dominant role of the HTS material cost due to the high excitation requirements. Generally, an approximately linear relation between the inverter's cost share and the generator active mass is found, irrespective of the considered topology. The largest contribution as well as the steepest relation are observed for the most cost-effective all-iron topology A, which offers the maximum potential of an overall cost decrease, if the HTS material price drops and more lightweight generators can be excited with a smaller HTS material investment.

Generators featuring topology D with stator air gap winding or generators A with all-iron rotor and slotted stator dominate the other topologies B and C regarding the system cost and the generators' active mass, Fig. 20b. Depending on the prioritisation of efficiency improvements and mass reduction (enabling e.g. a cheaper basement and tower structure of the wind power station) on one hand or minimum generator investment costs on the other hand, either topology A or D proves advantageous. In contrast, topologies B and C with partially or entirely non-magnetic rotor structure fall short with respect to technical and economical criteria.

5 Conclusions

7 MW partially superconducting direct drive synchronous generators with inner rotor high temperature superconducting DC excitation winding and AC poly-phase copper stator winding are compared for four different iron topologies A…*D*, comprising an all-iron design A, partially and entirely non-magnetic rotor structures (B and C) as well as either a slotted stator or a stator air gap winding (D). The study covers two different HTS tape characteristics as well as the influence of geometric restrictions on the generator's installation space, implying different electromagnetic utilisation C_e. The generator designs are optimised by means of a multi-objective numerical optimisation with 8 design parameters f_i, $i = 1, \ldots, 8$ that relies on non-linear FEM simulations in an iterative procedure. A thermal model and a cost model allow for an economical assessment of the variants including the cryogenic cooling system and the full inverter.

Generator designs D with stator air gap winding prove technically advantageous in terms of maximum efficiency and power factor. Current HTS material prices lead however to higher system costs due to the significantly increased excitation requirements. This topology still constitutes an attractive solution, if tapes with high-field performance due to APC) would be available at reduced prices < 100 €/kAm. To date, designs with all-iron topology A and a slotted stator prove superior, compared to partially or entirely non-magnetic rotor structures B and C. For this topology A, a major influence of the outer diameter restriction on efficiency, power factor, active mass and needed HTS tape quantity is identified, while the generator volume V_g has little influence. The cost share of the cryogenic cooling system is estimated to be less than 15% in case of a HTS operating temperature of $T = 30\,K$. For current HTS tape prices, the reduction of the cryogenic operating temperature to 20…25 K is a suitable measure to reduce the overall system cost in spite of the higher cooling requirements. The largest cost contribution of the full inverter is found for an all-iron topology A whereas the cost share is below 10% for all lightweight generator designs, irrespective of the topology (A…D).

Acknowledgements The authors would like to thank Stiftung Energieforschung Baden-Württemberg for the financial support.

Funding Open Access funding enabled and organized by Projekt DEAL.

References

1. Abrahamsen AB et al (2018) Comparison of Levelized cost of energy of superconducting direct drive generators for a 10-MW offshore wind turbine. IEEE Trans Appl Supercond 28(4):1–5
2. Advanced Research Systems (2022) ARS Cryocooler Series (Accessed on: 23. Nov. 2022) . https://www.arscryo.com/
3. Bergen A et al (2019) Design and in-field testing of the world's first ReBCO rotor for a 3.6 MW wind generator. Supercond Sci Technol 32:125006
4. Esson WB (1891) Der Entwurf multipolarer Dynamos. ETZ 27:355–356

5. Fujikura (2019) Introduction of FUJIKURA RE-based HTS Wire (Accessed on: 23. Nov. 2022). http://www.fujikura.co.jp
6. Karmaker MH, Kulkarni D (2015) Comparison between different design topologies for multi-megawatt direct drive wind generators using improved second generation high temperature superconductors. IEEE Trans Appl Supercond 25:5201605
7. Haran KS et al (2017) High power density superconducting rotating machines—development status and technology roadmap. Supercond Sci Technol 30:123002
8. Ingeteam (2021) Power converters – ready for your LcoE optimization (Accessed on: 20. Nov. 2022). https://www.ingeteam.com/
9. Köster R, Binder A (2022) Eddy current loss estimation for direct drive wind turbine generators with superconducting excitation winding by numerical and analytical models. Int J Numer Model e3066:1–13
10. Köster R, Binder A (2022) Multi-objective optimization of a direct-drive wind turbine generator with HTS excitation winding. IEEE Trans Appl Supercond 32(4):1–8
11. Lengsfeld S et al (2022) Comparing armature windings for a 10 MW fully superconducting synchronous wind turbine generator. In: 12th international conference on power, energy and electrical engineering (CPEEE), pp 49–53
12. Liu D (2017) Increasing the feasibility of superconducting generators for 10 MW direct-drive wind turbines. TU, Delft (Diss)
13. Liu D et al (2016) Comparison of superconducting generators and permanent magnet generators for 10-MW direct-drive wind turbines. In: 19th International Conference on Electrical Machines and Systems (ICEMS), pp 1–6
14. Liu Y, Qu R, Wang J (2014) Comparative analysis on superconducting direct-drive wind generators with iron teeth and air-gap winding. IEEE Trans Appl Supercond 24(3):1–5
15. Meeker DC (2018) J finite element method magnetics, version 4.2 (Accessed on: 13. Feb. 2022). https://www.femm.info
16. Nam G-D, Sung H-J, Go B-S, Park M, Yu I-K (2018) Design and comparative analysis of mgB2 and YBCO wire-based-superconducting wind power generators. Ieee Trans Appl Supercond 28(3):1–5
17. Nam G-D, Sung H-J, Go B-S, Park M, Yu I-K (2018) Design and comparative analysis of mgB2 and YBCO wire-based-superconducting wind power generators. Ieee Trans Appl Supercond 28(3):1–5
18. Polinder H et al (2013) Trends in wind turbine generator systems. IEEE J Emerg Sel Topics Power Electron 1(3):174–185
19. Saruwatari M et al (2016) Design study of 15-MW fully superconducting generators for offshore wind turbine. IEEE Trans Appl Supercond 26(4):1–5
20. Shi Cryogenics Group (2022) Cryocoolers product overview (Accessed on: 23. Nov. 2022). https://www.shicryogenics.com/
21. Siemens Gamesa (2022) SWT-7.0-154 offshore wind turbine (Accessed on: 20. Nov. 2022). https://www.siemensgamesa.com/products-and-services/offshore/wind-turbine-swt-7-0-154
22. Song X et al (2019) Designing and basic experimental validation of the world's first MW-class direct-drive superconducting wind turbine generator. IEEE Trans Energy Convers 34:2218–2225
23. Song X, Mijatovic N, Jensen BB, Holbøll J (2015) Design study of fully superconducting wind turbine generators. IEEE Trans Appl Supercond 25(3):1–5
24. Theva (2019) THEVA pro-line HTS wire – general properties (Accessed on: 07. Jan. 2020). https://www.theva.com/products/
25. Theva (2021) THEVA introduces superconductor with record performance for magnetic field applications, press release (Accessed on: 20. Nov. 2022). https://www.theva.de/wp-content/uploads/2021/08/PI_Hochfeldleiter-200821_en.pdf
26. Voestalpine Steel Division (2018) Electrical steel isovac high-perm 470-65 A – data sheet (Accessed on: 17. Jan. 2020). https://www.voestalpine.com/
27. Winergy (2022) Winergy generator – Wind is our element (Accessed on: 23. Nov. 2022). https://www.winergy-group.com/
28. Zhang Y, Cheng Y, Fan X, Li D, Qu R (2021) Electromagnetic fault analysis of superconducting wind generator with different topologies. Ieee Trans Appl Supercond 31(5):1–6

Robin Köster, M.Sc. Electrical Engineering, M.Sc. Industrial Engineering and M.Sc. Physics, Technical University Darmstadt in 2018, 2019 and 2020; since 2019 research assistant at the Institute of Electrical Energy Conversion, TU Darmstadt; field of research: electrical machines, especially synchronous generators for wind turbines and electrical machines with superconducting windings.

Andreas Binder, Diploma and doctoral degree in electrical engineering, Vienna University of Technology, Austria; 1981 to 1983 ELIN-Union AG, Vienna, development engineer; 1983 to 1989 researcher at the Institute of Electrical Machines and Drives, Vienna University of Technology; 1989 to 1997 Siemens AG, Bad Neustadt and Erlangen, group leader in motor and drive development; since 1997 Head of the Institute of Electrical Energy Conversion, Technical University of Darmstadt, as full professor; 2007 Medal of Honor of the ETG/VDE; Senior Member IEEE, member VDE, IET, VDI, EPE.